Volume 19, Number 1, 2026. pp. 13-22

Jordan Journal of Physics

ARTICLE

Synthesis and Characterization of Carbon Nanoporous Matrix Enriched with Nickel Oxide and Silica Nanoparticles for Glucose Sensor Applications

F. Sayari[a], N. Ben Mansour[a], M. Hjiri[b], G. Neri[c] and L. El Mir[a]

[a] *Laboratory of Physics of Materials and Nanomaterials Applied at Environment (LaPhyMNE), Gabes University, Faculty of Sciences of Gabes, 6072 Gabes, Tunisia.*

[b] *Department of Physics, College of Sciences, Imam Mohammad Ibn Saud Islamic University (IMSIU), Riyadh 11623, Saudi Arabia.*

[c] *Department of Engineering, University of Messina, 98166 Messina, Italy.*

DOI: **https://doi.org/10.47011/19.1.2**

Received on: 05/11/2024; *Accepted on: 13/08/2025*

Abstract: Nickel oxide (NiO) and silica (SiO_2) nanoparticles were incorporated into a carbon nanoporous matrix based on a pyrogallol-formaldehyde (PF) matrix via the sol-gel method. Various characterization techniques were performed to investigate the PF matrix, PF:NiO and PF/SiO_2:NiO nanocomposites. XRD patterns revealed broad peaks characteristic of amorphous SiO_2 and carbon phases characteristic of both amorphous SiO_2 and carbon phases along with three characteristic nickel (Ni) peaks in the two nanocomposites PF:NiO and PF/SiO_2:NiO. SEM images showed a significant number of particles covering the PF matrix surface in the PF/SiO_2:NiO nanocomposite. The TEM images confirmed the porous structure of the PF matrix, a uniform dispersion of Ni nanoparticles in the PF:NiO nanocomposite and notable nanoparticle agglomeration in the PF/SiO_2:NiO nanocomposite. Electrochemical measurements demonstrated that the sensitivity of the non-enzymatic glucose sensor increases with decreasing specific surface area. The electrical conductivity of the materials was found to depend on pore volume, decreasing as pore volume increased. The PF/SiO_2:NiO nanocomposite exhibited promising performance as a non-enzymatic glucose sensor with a sensitivity of 585 $\mu A \cdot mM^{-1} \cdot cm^{-2}$ and a low electrical conductivity of approximately 10^{-8} $\Omega^{-1} \cdot cm^{-1}$.

Keywords: Carbon nanoporous matrix, Nanocomposites, Nickel oxide, Silica, Non-enzymatic glucose sensor, Electrical conductivity.

Introduction

Nanoporous materials have attracted great attention due to their excellent properties when compared to conventional carbon materials. Indeed, their nanometric pore size, high specific surface area, and large pore volume enable their use in various applications, such as supercapacitor electrodes, gas storage, and as support for electrochemical sensors [1-4]. Carbon/Silica (C/SiO_2) nanocomposites have attracted attention for specific applications, such as in adsorption, electrodes, and cancer immunotherapy [5-7]. The high surface energy of SiO_2 nanoparticles facilitates the formation of grafting sites for other added elements [8]. Several synthetic routes have been developed for the production of C/SiO_2 nanocomposites [9-11]. In recent years, one of the most attractive research areas in the realm of sensors is the non-enzymatic glucose sensor. Electrochemical sensors are the most straightforward, reliable, fast, sensitive and cost-effective [12-14]. Among these sensors are those based on nanoparticles of transition metal oxides dispersed in a porous carbon matrix [15, 16]. Ni nanoparticles were selected due to their high surface-to-volume ratio, significant chemical stability and rapid electron conduction [17-19]. Ni-based hybrid nanocomposites have gained significant attention

Corresponding Author: Nabil Ben Mansour **Email**: Nabil.Benmansour@fsg.rnu.tn

due to their excellent electrocatalytic activity for glucose oxidation and their ability to enhance the electrical conductivity of organic matrices [20, 21]. SiO_2 nanoparticles are widely used to immobilize various biomolecules, due to their large specific surface area and strong surface-binding capabilities [22, 23]. However, when used alone within an organic matrix, SiO_2 nanoparticles are not ideal for constructing glucose sensors. Conversely, incorporating silica into an organic nanoporous matrix significantly enhances its stability, thereby improving the thermal and mechanical properties of the resulting hybrid material [24, 25]. Moreover, SiO_2 effectively fills the nanopores and provides a stable platform for the uniform distribution of nickel nanoparticles on the surface. This optimized structural arrangement substantially improves the glucose sensing performance of the nanocomposite sensor.

Electrical conductivity and non-enzymatic glucose sensing are typically highly influenced by the composition and morphology of the materials used [26-29]. In fact, metallic nanostructures, which exhibit high electrocatalytic activity for the oxidation of glucose [30, 31], enhance the active surface area and thus improve the electrocatalytic performance of glucose sensors when distributed on porous surfaces. The type of nanostructures, however, alters electrical conductivity; insulating nanostructures reduce it, whereas metal nanostructures increase it. In this study, the C/SiO_2 nanocomposite was prepared by incorporating SiO_2 nanoparticles into a carbon nanoporous matrix based on PF using the sol-gel method. The addition of Ni nanoparticles influenced the enhancement of various properties of the PF/SiO_2 nanocomposite. Indeed, the significant electrical conductivity, as well as the size and shape of these particles can modify the different properties of the final nanocomposite. Nevertheless, the interaction between Ni nanoparticles and the matrix promotes strong van der Waals forces, which facilitate good dispersion of the particles [32, 33].

The aim of this work is to investigate the impact of incorporating inorganic nanoparticles (NiO and SiO_2) on the structural, morphological, electrical, and electrochemical properties of the PF matrix. Special emphasis is placed on electrical conductivity and glucose sensing performance. The functional properties are examined in relation to key textural parameters, including specific surface area and pore volume, in order to gain deeper insight into how material texture influences charge transport and sensor efficiency.

2. Experimental Procedure

The sol-gel method was used for the synthesis of the materials. This process generally follows the steps illustrated in Fig. 1. First, a solution is prepared from precursors, typically alkoxides or metal salts mixed with a solvent. These precursors undergo polymerization through hydrolysis and condensation reactions to form a gel. Once the gel is formed, the material is subjected to an aging phase to enhance its lattice structure. The final drying step can be performed either under supercritical conditions to produce an aerogel, such as in the preparation of NiO and SiO_2 nanoparticles, or through conventional drying to obtain a xerogel, as is the case for the PF, PF:NiO and PF/SiO_2:NiO xerogel materials. In this study, SiO_2 and NiO nanoparticles were synthesized separately using tetraethoxysilane (TEOS) and nickel (II) chloride ($NiCl_2$, $6H_2O$) as precursors, respectively. In the first step, SiO_2 nanoparticles were obtained by mixing 15 ml of TEOS precursor with 21 ml of ethanol as the solvent and 8 ml of hydrofluoric acid as a catalyst. Separately, NiO nanoparticles were synthesized by dissolving 2 g of the $NiCl_2$,$6H_2O$ precursor in 14 ml of methanol. The solutions were subjected to magnetic stirring for 15 min and placed in an autoclave under supercritical ethanol conditions (T_c = 250 °C, P_c = 7 MPa) to extract the solvent. In the second step, the PF organic matrix was prepared using the sol-gel method according to Ben Mansour et al. [17-19]. NiO nanoparticles were incorporated into the PF matrix at a 5% mass ratio to yield the PF:NiO solution. To obtain the PF/SiO_2:NiO solution, SiO_2 and NiO nanoparticles were incorporated into the PF matrix at mass ratios of 20% and 1%, respectively. To obtain the wet gel, the solutions were desiccated in an open atmosphere at 50° C for 12 days to ensure a controlled and gradual evaporation rate, which minimizes the risk of crack formation. Afterwards, these gels were dried in an oven at a rate of 10 °C/day up to 150° C to get the PF, PF:NiO and PF/SiO_2:NiO xerogels. Finally, these xerogels were treated at 650 °C under inert atmosphere for 2 hours in a tubular furnace to acquire the PF matrix, PF:NiO and PF/SiO_2:NiO nanocomposites.

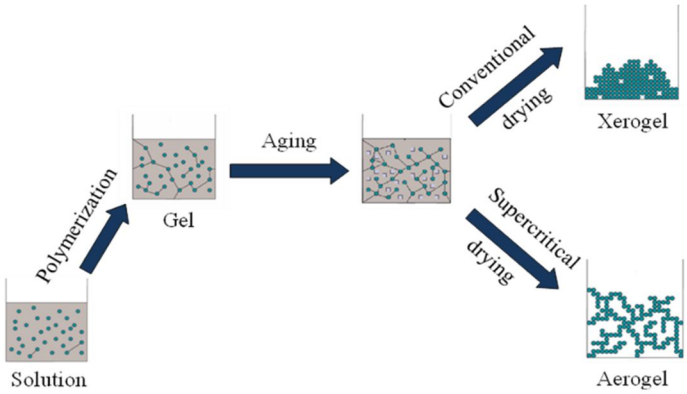

FIG. 1. The different steps of the sol-gel method.

3. Characterization

The synthesized powder materials were characterized using a MiniFlex series of benchtop X-ray diffractometer (XRD) with a Cu-Kα radiation equipped with a graphite monochromator, Field Emission Gun-Scanning Electron Microscopy (FEG-SEM, JSM-7600F), Transmission Electron Microscopy (TEM, FEI, Tecnai G2, F30) and X-ray Photoelectron Spectroscopy (XPS, Kratos Analytical, UK; SHIMADZU group) utilizing an Al-Kα radiation source. The electrochemical behavior was examined in the presence and absence of glucose using a DropSensStat 400 potentiostat/ galvanostat in 0.1 M KOH solution over a potential range of 0-1 V and at a scan rate of 50 $mV \cdot s^{-1}$. Conductivity measurements were performed using an Agilent 4294 impedance analyzer at room temperature.

4. Results and Discussions

Figure 2 shows the XRD diffractograms of PF matrix, PF:NiO and PF/SiO_2:NiO nanocomposites. Broad bands centered around 22° and 44° correspond to amorphous carbon and SiO_2 phases [34]. A series of well-defined peaks at 2θ values of approximately 44°, 51° and 76° are observed, corresponding to the (111), (200) and (220) planes of Ni structure in the PF:NiO and PF/SiO_2:NiO nanocomposites. These results indicate that NiO was reduced to Ni during pyrolysis at 650 °C [18, 19]. In contrast, SiO_2 typically requires much higher temperatures to be reduced to metallic silicon [35]. The JCPDS cards: JCPDS 01-1260, JCPDS 29-0085 and JCPDS 22-1069 correspond to Ni, graphite and SiO_2, respectively. The crystallite size of different samples was calculated from the Scherrer's equation - Eq. (1) [36]:

$$G = \frac{0.9\,\lambda}{B\cos\theta_B} \qquad (1)$$

where λ is the XRD wavelength (1.78901 Å), θ_B is the Bragg angle and B is the peak width at half maximum. Using Eq. (1), the average value of Ni crystallites is equal to 40 nm for PF:NiO nanocomposite and 38 nm for PF/SiO_2:NiO nanocomposite.

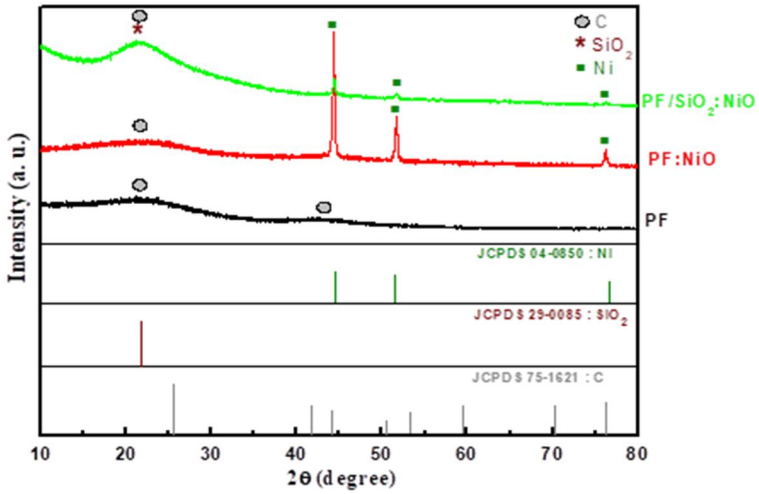

FIG. 2. XRD diffractograms of different samples.

The SEM images of the different samples are shown in Fig. 3. The compact layers of carbon particles observed in Fig. 3(a), along with visible voids between them, reflect the inactive surface and the porous texture of the PF matrix. For the PF:NiO nanocomposite (Fig. 3(b)), Ni particles appear to be randomly dispersed within the carbon matrix. In contrast, in the PF:NiO/SiO_2 nanocomposite (Fig. 3(c)), a greater number of particles are observed covering the carbon matrix surface compared to the PF:NiO nanocomposite. In this case, the SiO_2 acts as a support on which metallic Ni particles are anchored. These observations suggest that the PF:NiO/SiO_2 nanocomposite has a larger active surface area than the PF:NiO nanocomposite.

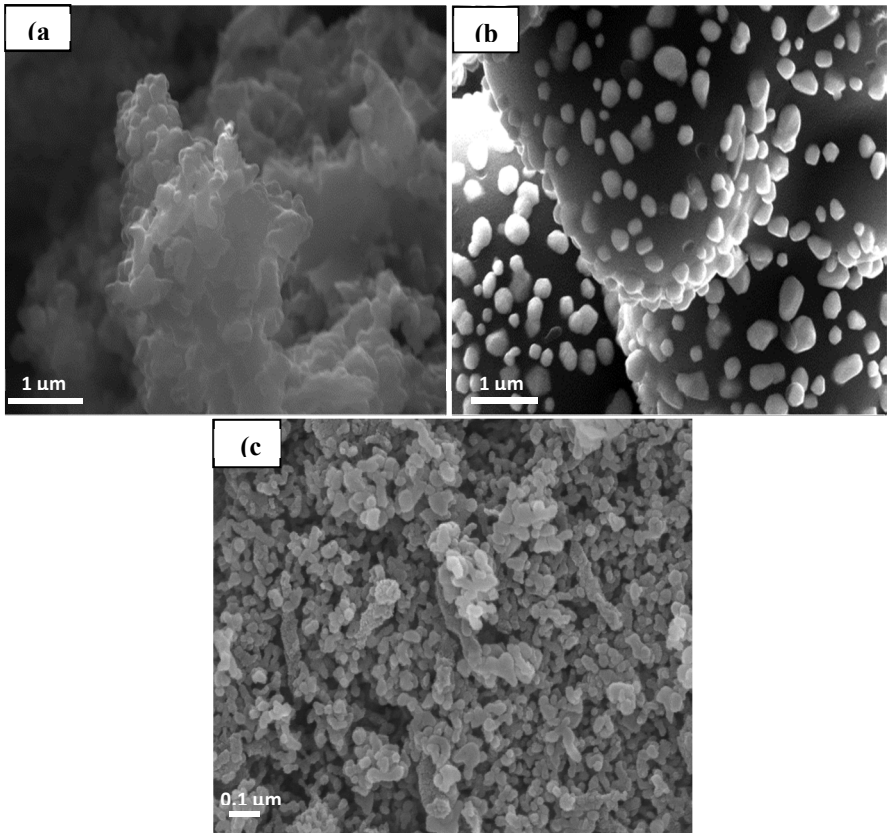

FIG. 3. SEM images of: (a) PF matrix, (b) PF:NiO nanocomposite and (c) PF/SiO_2:NiO nanocomposite.

The elemental composition of the materials was analyzed by energy-dispersive X-ray spectroscopy (EDX) coupled with a scanning electron microscope. The mass percentages of oxygen, silicon, carbon and nickel in the various samples are summarized in Table 1. For the PF matrix, the mass percentages of C and O are 98.28% and 1.72%, respectively. In the PF:NiO nanocomposite, the contents of C, O and Ni are 77.67%, 14.7% and 7.63%, respectively. In the PF/SiO_2:NiO nanocomposite, the measured mass percentages are 26.82% for C, 46.72% for O, 25.36% for Si and 1.1% for Ni.

TABLE 1. Surface elemental concentration of various samples

Sample	C (wt.%)	O (wt.%)	Ni (wt.%)	Si (wt.%)
PF	98.28	1.72	-	-
PF:NiO	77.67	14.7	7.63	-
PF/SiO_2:NiO	26.82	46.72	1.1	25.36

Figure 4 presents the XPS spectra of the studied materials. The spectrum of the PF matrix mainly exhibits a C 1s peak centered at around 282.5 eV, which is characteristic of carbon, along with a weak O 1s peak indicating the presence of oxygen-containing functional groups. For the PF:NiO nanocomposite, the appearance of a Ni 2p peak at 858 eV confirms the presence of nickel species. In the PF/SiO_2:NiO nanocomposite, in addition to the C 1s, Ni 2p and O 1s peaks, two distinct silicon peaks, Si 2p at 101.5 eV and Si 2s at 152.2 eV, are observed, confirming the presence of SiO_2 nanoparticles.

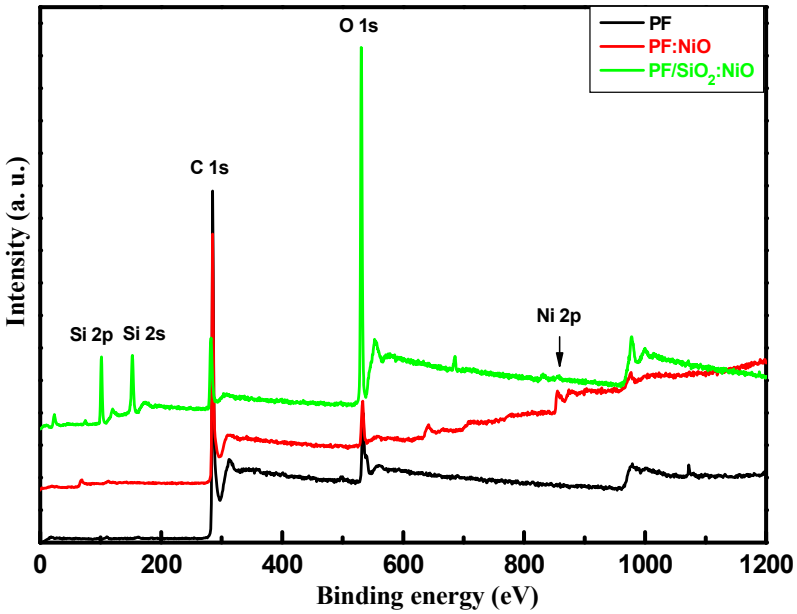

FIG. 4. XPS spectra of different samples.

The TEM image of the PF matrix (Fig. 5(a)) shows the microporous texture of this material. The average pore size (2 nm), specific surface area (720 m^2/g), and pore volume (0.33 cm^3/g) were calculated using the Brunauer-Emmett-Teller (BET) method [37]. The incorporation of the nanoparticles into the PF matrix reduced its porosity (Fig. 5(b) and 5(c)). In fact, the added nanoparticles filled the pores. This was clearly observed in the PF/SiO_2:NiO nanocomposite (Fig. 5(c)) where noticeable agglomerations of different types of particles are observed.

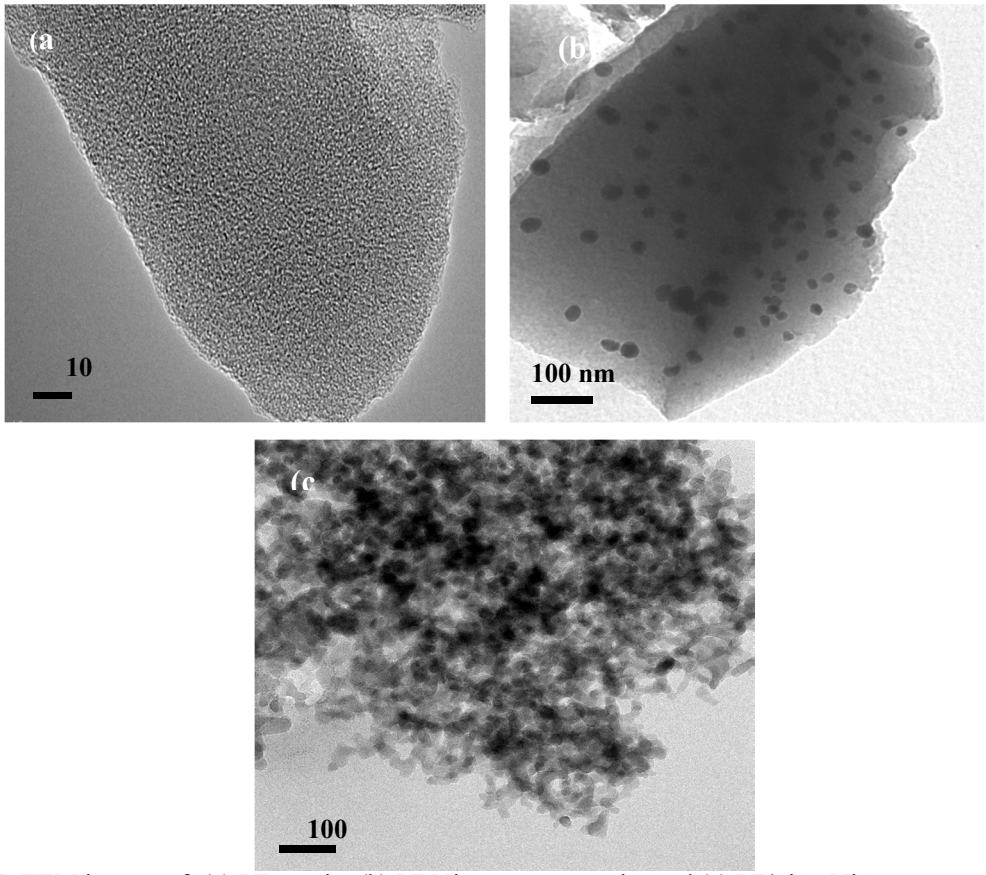

FIG. 5. TEM images of: (a) PF matrix, (b) PF:NiO nanocomposite and (c) PF/SiO_2:NiO nanocomposite.

The values of pore size, specific surface area and pore volume of the different samples, determined from our own BET measurements, are presented in Table 2 [37, 38]. These results confirm the decrease in specific surface area and pore size in the PF:NiO/SiO_2 nanocomposite, along with an increase in pore volume.

TABLE 2. Values of the specific surface area, pore volume and pore size for the different samples.

Samples	Specific surface area (m^2/g)	Pore volume (cm^3/g)	Pore size (nm)
PF	720	0.33	1.9
PF:NiO	461	0.22	2.6
PF/SiO_2:NiO	163	1.55	1.4

The electrochemical analysis of the different samples for glucose oxidation was conducted using cyclic voltammetry at a scan rate of 50 $mV.s^{-1}$ with 5 mM glucose present in 0.1 M KOH solution. The cyclic voltammetry results for PF matrix, PF:NiO and PF/SiO_2:NiO nanocomposites in the presence and absence of 5 mM glucose are displayed in Fig. 6. The lack of anodic or cathodic peaks in the PF matrix suggests that the carbon matrix exhibits minimal electrocatalytic activity towards glucose oxidation. Conversely, both in the presence and absence of glucose, the PF/NiO and PF/SiO_2:NiO nanocomposites display two oxidation and reduction peaks. These are caused by the electrochemical redox reaction of the Ni^{2+}/Ni^{3+} pair on the electrode surface [39, 40]. Specifically, upon applying a potential, metallic nickel (Ni^0) is first oxidized to nickel hydroxide ($Ni(OH)_2$) and then further oxidized to Ni^{3+}, forming oxyhydroxide species as described in Eq. (2) and Eq. (3), respectively:

$$Ni + 2OH^- \rightarrow Ni(OH)_2 + 2e^- \quad (2)$$

$$Ni(OH)_2 + OH^- \rightarrow NiOOH + H_2O + e^- \quad (3)$$

The resulting NiOOH serves as the active site for the electrochemical oxidation of glucose. In this process, glucose is oxidized to glucolactone in the presence of NiOOH as shown in Eq. (4):

$$NiOOH + \text{glucose} \rightarrow Ni(OH)_2 + \text{glucolactone} \quad (4)$$

Thus, this catalytic cycle relies on the rapid and reversible conversion between Ni^{2+} and Ni^{3+}, which facilitates efficient electron transfer.

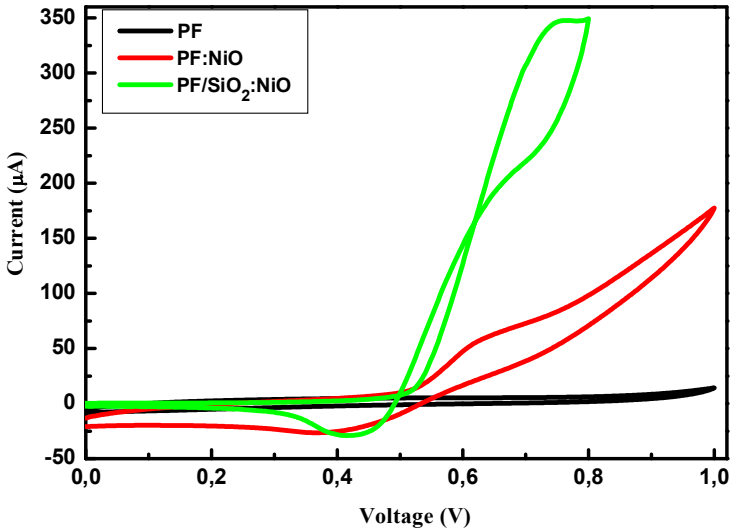

FIG. 6. Cyclic voltammograms in 0.1 M KOH with 5 mM glucose at a scan rate of 50 $mV.s^{-1}$.

The calibration curves for the PF:NiO and PF/SiO_2:NiO nanocomposites in 0.1 M KOH are shown in Fig. 7. The addition of glucose to the solution resulted in a noticeable increase in current for the PF/SiO_2:NiO nanocomposite. The sensitivity, calculated from the linear relationship between current and glucose concentration within the 0.05 mM to 1.5 mM range is equal to 76 $\mu A \cdot mM^{-1} \cdot cm^{-2}$ for the PF:NiO nanocomposite and approximately 585 $\mu A \cdot mM^{-1} \cdot cm^{-2}$ for the PF/SiO_2:NiO nanocomposite. The sensors exhibit detection limits of 0.01 mM for the PF:NiO nanocomposite with a response time of 1.9 s and 0.03 mM for the PF/SiO_2:NiO nanocomposite with a response time of 0.7 s based on a signal-to-noise ratio (S/N) of 3. The presence of SiO_2 in the PF/SiO_2:NiO nanocomposite improves the

dispersion of Ni nanoparticles as well as the mechanical and chemical stability of the material. This results in an increase in the electroactive surface area of the sensor, thus providing better performance than the PF:NiO nanocomposite. The efficiency of the PF/SiO_2:NiO nanocomposite for non-enzymatic glucose detection is comparable to those reported in the literature. Koyakutty et al. achieved a glucose detection sensitivity of 696 $\mu A \cdot mM^{-1} \cdot cm^{-2}$ using Ni/NiO-graphene heterostructures [41]. Marini et al. reported a sensitivity of 670 $\mu A \cdot mM^{-1} \cdot cm^{-2}$ for a carbon/nickel nanocomposite containing 30% nickel [42]. Yuan et al. obtained a sensitivity of 285 $\mu A \cdot mM^{-1} \cdot cm^{-2}$ in their study of Ni/silicon oxide/nitrogen-doped carbon nanocomposites [43].

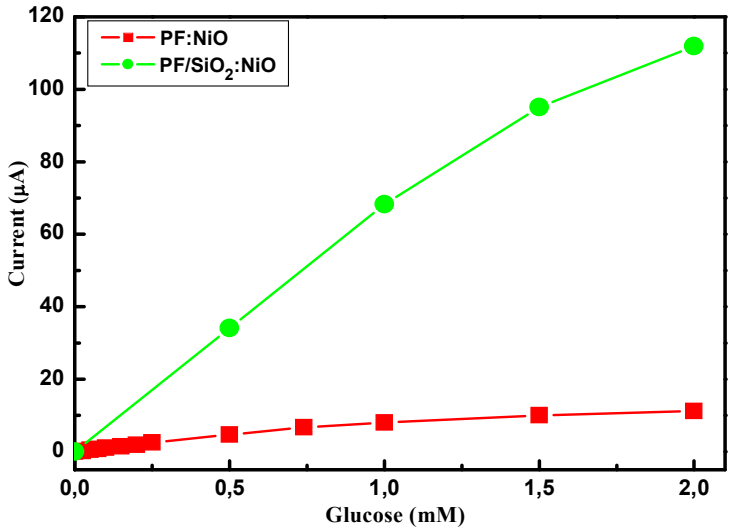

FIG. 7. Calibration curves of PF:NiO and PF/SiO_2:NiO nanocomposites at various glucose concentrations.

Figure 8(a) shows the chronoamperometric response recorded for successive additions of glucose for the PF/SiO_2:NiO nanocomposite. A noticeable improvement in the current response is observed after each glucose addition. The sensor selectivity was assessed, since it plays a crucial role in determining its effectiveness in real-world applications. In practical samples, glucose often coexists with other compounds such as sucrose, mannose, fructose, uric acid (UA), dopamine (DA) and ascorbic acid (AA). Fig. 8(b) illustrates the amperometric response of the PF/SiO_2:NiO nanocomposite-based sensor during successive additions of 1 mM glucose, 0.1 mM ascorbic acid, 0.1 mM uric acid, 0.1 mM dopamine and a second addition of 1 mM glucose. The results indicate that these electroactive species have minimal impact on the glucose detection signal, confirming that the sensor can selectively detect glucose even in complex physiological environments.

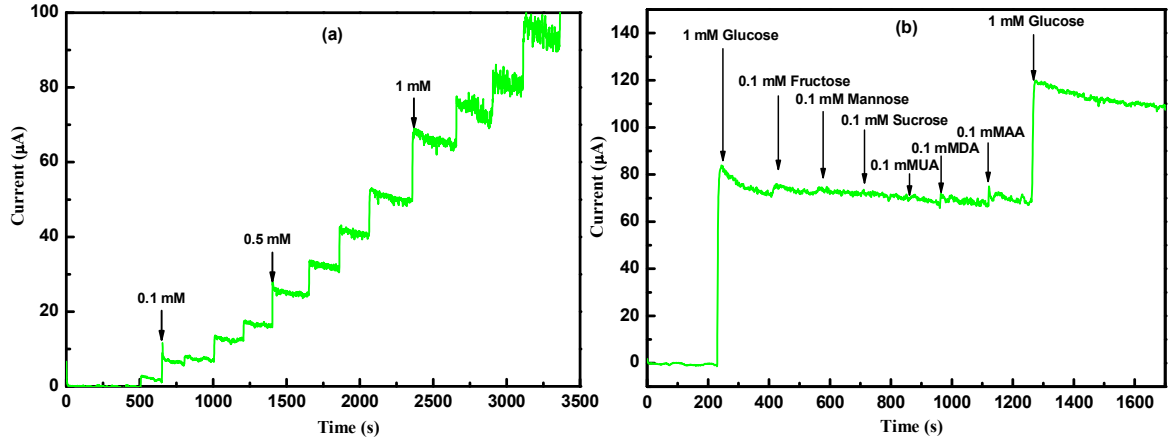

FIG. 8. Chronoamperometric response of the PF/SiO_2:NiO nanocomposite: (a) successive additions of glucose and (b) additions of glucose and interfering substances.

Figure 9 shows the variation in glucose detection sensitivity and specific surface area for the different samples. Generally, materials with a higher specific surface area provide more active sites, leading to increased sensitivity, as reported in the literature [44, 45]. In our study, according to Fig. 9, it is evident that the specific surface area is inversely proportional to the sensor sensitivity. Indeed, in these materials based on porous carbon, the performance mainly depends on the nature and accessibility of the active catalytic sites, rather than the specific surface area. In the PF matrix, despite its high specific surface area, the low electrochemical activity of carbon limits the sensitivity. Upon the addition of NiO nanoparticles, as in the PF:NiO nanocomposite, the specific surface area slightly decreases, but the presence of catalytically active nickel sites significantly enhances sensitivity. In the PF/SiO_2:NiO nanocomposite, the specific surface area is further reduced due to a denser structure. Nevertheless, the uniform dispersion of nickel particles, promoted by SiO_2, enables better electrochemical efficiency, resulting in the highest sensitivity. Therefore, in these sensors, the quality and distribution of active sites outweigh the role of specific surface area.

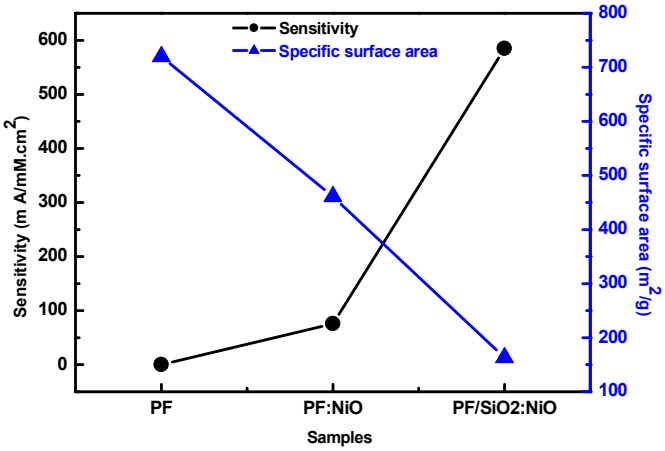

FIG. 9. Correlation between glucose detection sensitivity and specific surface area for the different samples.

The electrical conductivity of different samples was measured on a bulk (monolithic) sample using the Eq. (5):

$$\sigma = \frac{e}{RS} \quad (5)$$

where e is the thickness, R is the resistance and S is the contact surface area with the electrodes. This volumetric measurement of conductivity indicates that the pore volume has an effect on the electrical conductivity of the studied materials. The variations in electrical conductivity and pore volume of the different samples are shown in Fig. 10. It is clear that the highest electrical conductivity corresponds to the smallest pore volume in the case of PF:NiO nanocomposite. The conductivity decreases as the pore volume increases, reaching its minimum in the PF/SiO_2:NiO nanocomposite which exhibits the largest pore volume. These results suggest that, in these PF-based materials, electrical conductivity is inversely proportional to the pore volume.

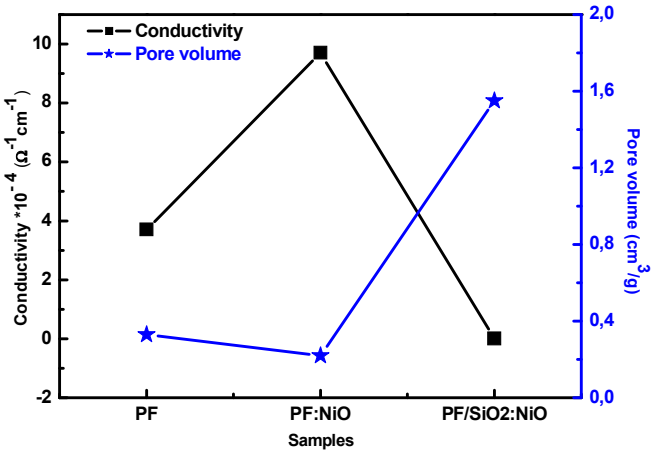

FIG. 10. Correlation between electrical conductivity and pore volume in the various synthesized samples.

5. Conclusions

This work investigated the influence of NiO and silica SiO_2 nanoparticles on the glucose detection performance and electrical conductivity for a nanoporous organic matrix based on pyrogallol-formaldehyde (PF). PF matrix, PF:NiO and PF/SiO_2:NiO nanocomposites were synthesized via the sol-gel process and subjected to pyrolysis at 650°C for two hours under an inert atmosphere. The specific surface area and the pore volume were found to affect, respectively, the glucose sensing sensitivity and the electrical conductivity. Structural and morphological characterizations explained these variations, showing that the glucose detection sensitivity is inversely proportional to the specific surface area, while electrical conductivity is inversely proportional to the pore volume. The highest glucose sensing sensitivity was observed for the PF/SiO_2:NiO nanocomposite, which exhibited the lowest electrical conductivity.

6. Acknowledgments

This study was supported by the project 21PEJC D1P20 (Programme d'Encouragement des Jeunes Chercheurs) funded by the Ministry of Higher Education and Scientific Research (Tunisia).

References

[1] Singh, K., Travlou, N.A., Bashkova, S., Castellón, E.R., and Bandosz, T.J., Carbon, 80 (2014) 183.

[2] Tolosa, A., Krüner, B., Jäckel, N., Aslan, M., Vakifahmetoglu, C., and Presser, V., Journal of Power Sources, 313 (2016) 178.

[3] Ben Mansour, N., Djeridi, W., and El Mir, L., Journal of Inorganic and Organometallic Polymers and Materials, 29 (1) (2019) 192.

[4] Shao, H., Wu, Y.C., Lin, Z., Taberna, P.L., and Simon, P., Chemical Society Reviews, 2020 (2020) 49.

[5] Scott, B.J., Wirnsberger, G., and Stucky, G.D., Chemistry of Materials, 13 (2001) 3140.

[6] Tsionsky, M., Gun, G., Glezer, V., and Lev, O., Analytical Chemistry, 66 (1994) 17473.

[7] Wang, H., Pan, X., Wang, X., Wang, W., Huang, Z., Gu, K., Liu, S., Zhang, F., Shen, H., Yuan, Q., and Liu, H., ACS Nano, 14 (2020) 2847.

[8] Qin, W., Vautard, F., Askeland, P., Yu, J., and Drzal, L.T., Polymer Composites, 38 (7) (2017) 1474.

[9] Shin, Y.S., Wang, C.M., and Exarhos, G.L., Advanced Materials, 17 (2005) 73.

[10] Guo, X.Y. and Jin, G., Journal of Materials Science, 40 (2005) 1301.

[11] Jankong, S. and Srikulkit, K., Journal of Metals, Materials and Minerals, 18 (2) (2008) 143.

[12] Baranwal, J., Barse, B., Gatto, G., Broncova, G., and Kumar, A., Chemosensors, 10 (9) (2022) 363.

[13] Lawal, A.T., Sensing and Bio-Sensing Research, 41 (2023) 100571.

[14] Arivazhagan, M., Saetang, S., Permwong, W., and Jakmunee, J., Electrochimica Acta, 507 (2024) 145148.

[15] Yu, D., Ying, W., Liang, S., Heng, Z., and Yu, L., Materials Chemistry, 20 (2010) 9918.

[16] Yang, J., Jiang, L.C., Zhang, W.D., Gunasekaran, S., Sensors & Actuators, B, 191 (2014) 86.

[17] Ben Mansour, N. and El Mir, L., Journal of Materials Science: Materials in Electronics, 27 (11) (2016) 11682.

[18] Ben Mansour, N. and El Mir, L., Solid State Sciences, 85 (2018) 38.

[19] Ben Mansour, N. and El Mir, L., Journal of Physics and Chemistry of Solids, 127 (2019) 1.

[20] Akter, R., Saha, P., Shah, S.S., Shaikh, M.N., Aziz, Md.A., and Ahammad, A.J.S., Chemistry and Asian Journal, 17 (23) (2022) 202200897.

[21] Maleh, H.K., Cellat, K., Arikan, K., Savk, A., Karimi, F., and Şen, F., Materials Chemistry and Physics, 250 (2020) 123042.

[22] He, P. and Hu, N., Electroanalysis, 16 (2004) 1122.

[23] He, P., Hu, N., and Rusling, J.F., Langmuir, 20 (2004) 722.

[24] Gao, T. and Jelle, B.P., Journal of Nanoparticle Research, 21 (2019) 108.

[25] AlSoud, A., Daradkeh, S.I., Knápek, A., Holcman, V., and Sobola, D., Physica Scripta, 98 (2023) 125520.

[26] Moghim, I., Rahsepar, M., Mousavi, S.M., Zangeneh, M., and Chiang, W.H., Microchemical Journal, 215 (2025) 114338.

[27] Yang, J., Yin, J., and Xu, L., Journal of Alloys and Compounds, 1010 (2025) 177796.

[28] Rezaei, A., Kamali, B., and Kamali, A.R., Measurement, 150 (2020) 107087.

[29] Mohsin, M.E.A. and Mousa, S., Polymers, 17 (4)(2025) 497.

[30] Liu, W., Chai, G., Zhao, X., Dai, Y., and Qi, Y., Sensors & Actuators B: Chemical, 321(2020) 128485.

[31] Liu, S., Wang, Z., Wang, F., Yu, B., and Zhang, T., RSC Advances, 4(2014) 33327.

[32] Dutta, N. and Green, D., Langmuir, 24 (10) (2008) 5260.

[33] Dasog, M. and Scott, R.W.J., Langmuir, 23 (6) (2007) 3381.

[34] Sarangi, M., Nayak, P., and Tiwari, T.N., Composites Part B: Engineering, 42(7) (2011) 1994.

[35] Lee, H.C., Dhage, S., Akhtar, M.S., Kwak, D.H., Lee, W.J., Kim, C.Y., and Yang, O.B., Current Applied Physics, 10 (2) (2010) S218.

[36] Saeki, H., Tabata, H., and Kawai, T., Solid State Communications, 120 (2001) 439.

[37] Ben Mansour, N., Djeridi, W., and El Mir, L., Journal of Inorganic and Organometallic Polymers and Materials, 29 (1) (2019) 192.

[38] Zahmouli, N., Marini, S., Guediri, M., Ben Mansour, N., Hjiri, M., El Mir, L., Espro, C., Neri, G., and Leonardi, S.G., Chemosensors, 6 (4) (2018) 54.

[39] Lu, M., Zhang, L., Qu, F.L., Lu, H.X., Zhang, X.B., Wu, Z.S., Huan, S.Y., Wang, Q.A., Shen, G.L., and Yu, Q.R., Biosensors & Bioelectronics, 25 (2009) 218.

[40] Tian, H., Jia, M., Zhang, M., and Hu, J., Electrochimica Acta, 96 (2013) 285.

[41] Koyakutty, H., Niranjana, J.S., and Bushiri, M.J., Materials Chemistry and Physics, 309 (2023) 128330.

[42] Marini, S., Ben Mansour, N., Hjiri, M., Dhahri, R., El Mir, L., Espro, C., Bonavita, A., Galvagno, S., Neri, G., and Leonardi, S.G., Electroanalysis, 30 (2018) 727.

[43] Yuan, M., Guo, X., Li, N., Li, Q., Wang, S., Liu, C.S., and Pang, H., Sensors and Actuators B: Chemical, 297 (2019) 126809.

[44] Kim, J.Y., Jo, S.Y., Sun, G.J., Katoch, A., Choi, S.W., and Kim, S.S., Sensors and Actuators B: Chemical B, 192 (2014) 216.

[45] Singh, S. and McShane, M., Biosensors and Bioelectronics, 26 (2011) 2478.